used.[11b] The absorption correction was applied by the Walker and Stuart method[11c] once a complete structural model was available and all atoms refined isotropically. Considering the extremely large absorption coefficient, the effect of the correction was dramatic, allowing not only a drop of ca. 15% of the R factor but also detection of the O atom disorder discussed above. Only the Os atoms, however, could be treated anisotropically.

Because of the disorder, the possibility that the structural model could be treated in the noncentrosimmetric space group Cc was also tested: after refinement by blocked full-matrix least squares the Os–Os bond lengths, related by the 2-fold axis in the space group $C2/c$, remained strictly equivalent, indicating that the static disorder was not an artifact of the centric refinement. Fractional atomic coordinates are reported in Table III.

Crystal Packing Investigation: Methodology. In our approach to crystal packing use is made of the expression ppe = $\sum_i\sum_j[A \exp(-Br_{ij}) - Cr_{ij}^{-6}]$, where ppe represents the packing potential energy[12a] and r_{ij} represents the nonbonded atom–atom intermolecular distance. Index i in the summation runs over all atoms of one molecule (chosen as the reference molecule), and index j, over the atoms of the surrounding molecules distributed according to crystal symmetry. A cutoff of 15 Å has been adopted in our calculations. The values of the coefficients A, B, and C used in this work have been taken from the literature[12b] and discussed in previous papers.[4] The results of ppe calculations are used to select the first-neighboring molecules (FNM) among the molecules surrounging the one chosen as reference (RM) on the basis of the contribution to ppe. It should be stressed that this procedure is used only as a convenient means to investigate the molecular environment within the crystalline lattice without pretentions of obtaining "true" (or even approximate) crystal potential energy values. All calculations were carried out with the aid of the computer program OPEC.[13] SCHAKAL88[14] was used for the graphical representation of the results.

Acknowledgment. Financial support by the Ministero della Università e della Ricerca Scientifica e Tecnologica is acknowledged; D.B., F.G., and B.F.G.J. wish also to acknowledge a collaborative research NATO grant.

Registry No. $[PPN]_2[Os_{10}C(CO)_{24}]$, 75117-74-7; $Os_3(CO)_{12}$, 15696-40-9; $H_2Os_{10}C(CO)_{24}$, 77908-36-2; Os, 7440-04-2.

Supplementary Material Available: Tables of anisotropic thermal parameters, fractional atomic coordinates and thermal parameters, and complete bonds and angles (9 pages); an F_o/F_c table (13 pages). Ordering information is given on any current masthead page.

(12) (a) Kitaigorodsky, A. I. *Molecular Crystal and Molecules*; Academic Press: New York, 1973. (b) Pertsin, A. J.; Kitaigorodsky, A. I. *The Atom-Atom Potential Method*; Springer-Verlag: Berlin, 1987. (c) Gavezzotti, A.; Simonetta, M. *Chem. Rev.* **1981**, *82*, 1. (d) Mirsky, K. *Computing in Crystallography, Proceedings of the International Summer School on Crystallographic Computing*; Delf University Press: Twente, The Netherlands, 1978; p 169.

(13) Gavezzotti, A. OPEC, Organic Packing Potential Energy Calculations. University of Milano, Italy. See also: Gavezzotti, A. *J. Am. Chem. Soc.* **1983**, *195*, 5220.

(14) Keller, E. SCHAKAL88, Graphical Representation of Molecular Models. University of Freiburg, FRG.

Crystal Construction and Molecular Interplay in Solid Ferrocene, Nickelocene, and Ruthenocene

Dario Braga* and Fabrizia Grepioni

Dipartimento di Chimica "G. Ciamician", Università di Bologna, Via Selmi 2, 40126 Bologna, Italy

Received September 20, 1991

The molecular organization in crystals of nickelocene, ruthenocene, and the monoclinic, orthorhombic, and triclinic modifications of ferrocene has been investigated by means of packing potential energy calculations and computer graphic analysis. The relationship between the various phases has been explored showing that small differences in molecular geometries and in intermolecular nonbonding interactions account for relevant differences in crystal properties. Potential energy barriers to ring reorientations have been calculated and compared with those obtained from anisotropic displacement parameters and from spectroscopic sources.

Introduction

Over the last 30 or 40 years a great deal of progress has been made in understanding the packing modes of molecules and the relationship between crystal packing and molecular shape. The occurrence of dynamic phenomena in molecular crystals has also been extensively investigated.[1] However, virtually all the work in this area has been on organic molecules,[2] leaving the neighboring field of organometallic solid-state chemistry almost totally unexplored. In an attempt to broaden this perspective we have recently begun an investigation of the molecular organization and of the recognition process which leads to the self-assembling of organometallic molecules in a crystal.[3] The dynamic behavior, from small-amplitude librations to large amplitude motions and reorientations of molecular fragments, shown by a number of neutral organometallic species in the solid state has also been studied.[4]

(1) Kitaigorodsky, A. I. *Molecular Crystal and Molecules*; Academic Press: New York, 1973.

(2) Gavezzotti, A.; Simonetta, M. In *Organic Solid State Chemistry*; Desiraju, G. R., Ed.; Elsevier: Amsterdam, 1987.

(3) (a) Braga, D.; Grepioni, F.; Sabatino, P. *J. Chem. Soc., Dalton Trans.* **1990**, 3137. (b) Braga, D.; Grepioni, F. *Acta Crystallogr., Sect. B* **1989**, *B45*, 378. (c) Braga, D.; Grepioni, F. *Organometallics* **1991**, *10*, 1254. (d) Braga, D.; Grepioni, F. *Organometallics* **1991**, *10*, 2563.

(4) (a) Braga, D.; Gradella, C.; Grepioni, F. *J. Chem. Soc., Dalton Trans.* **1989**, 1721. (b) Braga, D.; Grepioni, F. *Polyhedron* **1990**, *1*, 53. (c) Braga, D.; Grepioni, F.; Johnson, B. F. G.; Lewis, J.; Martinelli, M. *J. Chem. Soc., Dalton Trans.* **1990**, 1847. (d) Aime, S.; Braga, D.; Gobetto, R.; Grepioni, F.; Orlandi, A. *Inorg. Chem.* **1991**, *30*, 951. (e) Braga, D.; Anson, C. E.; Bott, A.; Johnson, B. F. G.; Marseglia, E. *J. Chem. Soc., Dalton Trans.* **1990**, 3517. (f) Anson, C. E.; Benfield, R. E.; Bott, A. W.; Braga, D.; Marseglia, E. *J. Chem. Soc., Chem. Commun.* **1988**, 889.

0276-7333/92/2311-0711$03.00/0

Chart I

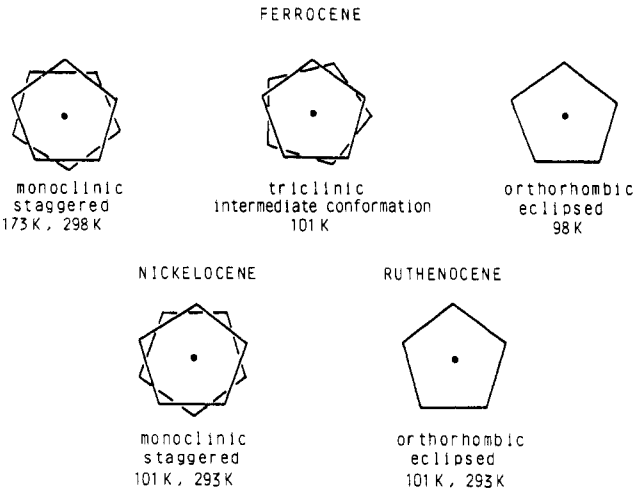

This paper is devoted to an analysis of the relationships between *crystal* and *molecular* structures of the metallocenes species $(C_5H_5)_2Fe$, $(C_5H_5)_2Ni$, and $(C_5H_5)_2Ru$.[5-9] These are fundamental molecules on which an extraordinary amount of experimental and theoretical work has already been done; the essential structural features are summarized in Chart I. The dynamic properties of these species in the solid state have also been the subject of much work[10-16] over the last two decades. In spite of these efforts, a few questions still remain unanswered.

(i) What is the relationship between the various crystal modifications of ferrocene (i.e. monoclinic with average staggered molecules, orthorhombic with eclipsed molecules, and triclinic with molecules in intermediate conformation)?

(ii) What is the reason for the different behavior of monoclinic ferrocene and nickelocene upon cooling? (I.e., why does ferrocene undergo a transition toward a triclinic phase at 164 K,[17] while nickelocene retains the monoclinic structure but shows a peculiar lengthening of the unit cell *b* axis on decreasing the temperature to 101 K?)

(iii) What is the relationship between the crystal structures of orthorhombic ferrocene and ruthenocene and between those of monoclinic ferrocene and nickelocene?

(iv) Finally, is it possible to relate the Cp ligand reorientational barriers calculated by means of the atom–atom pairwise potential energy method to the activation energies/potential barriers detected by various spectroscopic methods[11-16] or obtained from the anisotropic displacement parameters[10] for these species?

In order to answer these questions we have chosen to apply to these systems methods and procedures previously developed to investigate the factors controlling the crystal packing of first-row transition-metal binary carbonyls and the relationship between the shape of metal-coordinated arene fragments and the molecular organization and dynamic behavior in the solid state.[3,4]

Methodology

Our approach to crystal packing has its roots in the atom–atom pairwise potential energy method[18] developed and still widely used in the field of organic solid-state chemistry.

In order to study the molecular organization in a crystal we focus our attention on the number and distribution of the first neighboring molecules around the molecule chosen as a reference (RM), so that the full translational symmetry of the crystal lattice is, in a sense, neglected. These molecules constitute the so-called "enclosure shell" (ES).[3] The ES features are not easily studied by "conventional" crystallographic methods, while they are easily accessible from potential energy calculations based on the atom–atom approach.[18] The packing potential energy (ppe) of a neutral organometallic crystal is evaluated by means of the expression $\text{ppe} = \sum_i\sum_j[A \exp(-Br_{ij}) - Cr_{ij}^{-6}]$ where r_{ij} represents the nonbonded atom–atom intermolecular distance. Index i in the summation runs over all atoms of the RM and index j over the atoms of the surrounding molecules distributed according to crystal symmetry. A cutoff of 10 Å has been adopted in our calculations. The values of the coefficients A, B, and C used in this work are taken from the literature[19] and have been reported in previous papers.[3,4] The metal atoms (Ni, Fe, and Ru) are treated as the corresponding noble gases (Kr and Xe). Ionic contributions are not considered to be important for the purposes of this study.

The ES molecules are selected among the molecules generated by space group symmetry around the RM (usually in number from 60 to 80 within the cutoff of 10 Å) on the basis of their contribution to ppe, making sure that all relevant contributions are taken into account. We have found that this strategy guarantees an exact knowledge of the immediate environment of the molecule under investigation and greatly simplifies the study of the intermolecular interactions. It should be stressed that ppe calculations have no pretension of obtaining "true" crystal potential energy values but provide a convenient means to investigate the packing relationship among the molecules. On these premises the following discussion on the various contributions to ppe (see next section) will be meaningful only on a relative basis. A complete listing of the symmetry operations which generate the ESs and of the individual contribution to ppe of each ES molecule for all species discussed herein is available as supplementary material.

All calculations were carried out with the aid of the computer program OPEC.[20] SCHAKAL88[21] was used for the graphical representation of the results.

In order to evaluate the potential energy barriers to reorientation, ppe values were calculated for different

(5) Seiler, P.; Dunitz, J. D. *Acta Crystallogr., Sect. B* **1982**, *B38*, 1741.
(6) Seiler, P.; Dunitz, J. D. *Acta Crystallogr., Sect. B* **1979**, *B35*, 2020.
(7) (a) Takusagawa, F.; Koetzle, T. F. *Acta Crystallogr., Sect. B* **1979**, *B35*, 1074. (b) Seiler, P.; Dunitz, J. D. *Acta Crystallogr., Sect. B* **1979**, *B35*, 1068.
(8) Seiler, P.; Dunitz, J. D. *Acta Crystallogr., Sect B* **1980**, *B36*, 2255.
(9) Seiler, P.; Dunitz, J. D. *Acta Crystallogr., Sect. B* **1980**, *B36*, 2946.
(10) Maverick, E.; Dunitz, J. D. *Mol. Phys.* **1987**, *62*, 451.
(11) Chhor, K.; Lucazeau, G.; Sourisseau C. *J. Raman Spectrosc.* **1981**, *11*, 183.
(12) Holm, C. H.; Ibers, J. A. *J. Chem. Phys.* **1959**, *30*, 885.
(13) (a) Campbell, A. J.; Fyfe, C. A.; Harold-Smith, D.; Jeffrey, K. R. *Mol. Cryst. Liq. Cryst.* **1976**, *36*, 1. Levendis, D. C.; Boyens, J. C. A. *J. Crystallogr. Spectrosc. Res.* **1985**, *15*, 1.
(14) Kubo, A.; Ikeda, R.; Nakamura, D. *Chem. Lett. Jpn.* **1981**, 1497.
(15) Gardner, A. B.; Howard, J.; Waddington, T. C.; Richardson, R. M.; Tomkinson, J. *Chem. Phys.* **1981**, *57*, 453.
(16) Sourisseau, C.; Dianoux, A. J.; Poinsignon, C. *Mol. Phys.* **1983**, *48*, 367.
(17) Edwards, J. W.; Kington, G. L.; Mason, R. *J. Chem. Soc., Faraday Trans.* **1959**, *55*, 660.
(18) Pertsin, A. J.; Kitaigorodsky, A. I. *The atom-atom potential method*; Springer-Verlag: Berlin, 1987.
(19) (a) Gavezzotti, A. *Nouv. J. Chim.* **1982**, *6*, 443. (b) Mirsky, K. *Computing in Crystallography, Proceedings of the International Summer School on Crystallographic computing*; Delft University Press: Twente, Netherlands, 1978; p 169. (c) Gavezzotti, A.; Simonetta, M. *Chem. Rev.* **1982**, *82*, 1.
(20) Gavezzotti, A. OPEC, Organic Packing Potential Energy Calculations. University of Milano, Italy, 1975. See also Gavezzotti, A. *J. Am. Chem. Soc.* **1983**, *195*, 5220.
(21) Keller, E. SCHAKAL88, Graphical Representation of Molecular Models. University of Freiburg, FRG, 1988.

Table I. Results of ppe Calculations for Ferrocene, Nickelocene, and Ruthenocene[a]

	ferrocene orthorhombic	ferrocene triclinic	ferrocene monoclinic	ferrocene monoclinic
T, K	98[5]	101[6]	173[7a]	293[7a]
sg, Z	*Pnma*, 4	*F*1, 16	$P2_1/a$, 2	$P2_1/a$, 2
V_{cell}, Å^3	766.5	3116	395	406.2
ppe	-38.3	-37.4	-37.7	-36.4
$\sum_{H\cdots H}$	-2.2	-1.9	-1.8	-2.0
$\sum_{C\cdots H}$	-10.5	-10.3	-11.4	-11.2
$\sum_{C\cdots C}$	-15.3	-15.2	-14.9	-14.2
$\sum_{Cp\cdots Cp,\ \%\ ppe}$	-28.0, 73	-27.4, 73	-28.1, 75	-27.4, 75
$\sum_{M\cdots M}$	-0.7	-0.6	-0.6	-0.6
$\sum_{M\cdots Cp}$	-9.6	-9.4	-9.0	-8.4
	nickelocene monoclinic		ruthenocene orthorhombic	
T, K	101[8]	293[8]	101[9]	293[9]
sg, Z	$P2_1/a$, 2	$P2_1/a$, 2	*Pnma*, 4	*Pnma*, 4
V_{cell}, Å^3	403.7	426.0	788.5	818.4
ppe	-37.6	-35.1	-43.0	-41.7
$\sum_{H\cdots H}$	-2.2	-2.1	-2.1	-2.2
$\sum_{C\cdots H}$	-10.9	-10.9	-10.5	-10.8
$\sum_{C\cdots C}$	-14.8	-13.5	-15.2	-14.4
$\sum_{Cp\cdots Cp,\ \%\ ppe}$	-27.9, 74	-26.5, 75	-27.8, 65	-27.4, 66
$\sum_{M\cdots M}$	-0.6	-0.5	-1.6	-1.4
$\sum_{M\cdots Cp}$	-9.1	-8.1	-13.6	-12.9

[a] $\sum_{X\cdots X}$ (kcal·mol^{-1}) represents the separate interatom or intergroup contributions to ppe.

conformations of the Cp fragments. These were rotated in steps of 10° about the axes passing through the metal atoms and the centers of mass of the ligands. The H-atom positions, when obtained by X-ray diffraction, were replaced by calculated ones based on a C–H distance of 1.08 Å. The potential energy barriers [ΔE(ppe)] were calculated as ΔE(ppe) = ppe − ppe(min) where ppe(min) are the values corresponding to the observed structures (0° rotation).

Results and Discussion

The results of ppe calculations and of the partitioning of the energy into the separate interatom and intergroup contributions together with some crystal qualifiers and the references to the original paper are reported in Table I. Given the caveat raised above on the reliability of ppe calculations in organometallic crystals, the following general observations can be made: (i) ppe magnitudes show a congruent inverse dependence on the temperature; (ii) ppe in orthorhombic ruthenocene is expectedly more "cohesive" than in ferrocene and nickelocene because of the presence of a second-row metal; (iii) orthorhombic ferrocene (98 K) is only slightly more stable than triclinic ferrocene at 101 K (0.9 kcal mol^{-1}); (iv) in monoclinic nickelocene and ferrocene, Cp···Cp interactions account for ca. 75% of the total ppe; this percentage contribution decreases to ca. 65% in ruthenocene; (v) Cp···Cp contributions fall in the narrow range −26.5 to −28.1 kcal mol^{-1}. Considering the approximate nature of ppe calculations, other small differences among the values listed in Table I cannot be confidently discussed.

Molecular Organization in the Monoclinic and Orthorhombic Forms of Ferrocene and a Possible Way To Look at the Phase Transition. The ES approach allows a direct investigation of the relationship between the monoclinic and orthorhombic phases of ferrocene. Orthorhombic ferrocene, though thermodynamically stable up to 242 K, can be obtained by crystallization from solution only below 110 K.[5] Once formed, orthorhombic ferrocene can be warmed to ca. 275 K before the transition to the monoclinic form occurs. The following

Chart II

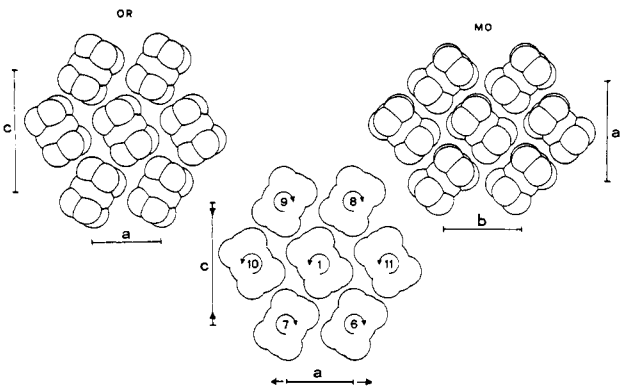

analysis will be based on the monoclinic structure at 173 K (from neutron diffraction data[7a]) and on the orthorhombic structure at 98 K (from X-ray diffraction data[5]). Before proceeding with the discussion, we would like to stress that we have no means to include in our modeling of the *crystal structure* of monoclinic ferrocene (and of nickelocene at room temperature) the presence of static disorder evidenced by the unsymmetrical pattern of the C-atoms adp's.[7b,8]

The ESs for the monoclinic (MO) and orthorhombic (OR) forms of ferrocene are shown in Figure 1a,b, respectively (but note that these are also the ESs of monoclinic nickelocene[8] and orthorhombic ruthenocene[9]). Both ESs consist of 14 molecules which account for 94.4% and 94.5% of the total ppe, respectively. The two outer layers of molecules are exactly superposed in the OR form, while they are shifted with respect to the central one in the MO form as sketched in Figure 1c,d, respectively. Partitioning of the ppe among these 14 molecules allows the following differences to be detected: (i) the six equatorial molecules surrounding the RM contribute ca. 43% and 33% of the total ppe in the MO and OR forms, respectively; (ii) consequently, the contribution of the molecules belonging to the outer layers is larger in the OR than in the MO form. This is reflected in the interlayer stacking distance which is shorter in the OR form [ca. 4.5 Å] than in the MO form [ca. 5.0 Å]; (iii) in both MO and OR forms the molecules with the largest contribution to ppe have their molecular axes parallel to those of the RMs. There are four such molecules in the OR form contributing ca. 50% of the total ppe (molecules 2–5 in Figure 1b). In the MO form, there are only two molecules (2 and 3 in Figure 1a), contributing ca. 25% of the ppe.

A section through the metal atom and parallel to the Cp rings of the RM reveals that, in both MO and OR forms, the Cp ligands of these close neighboring parallel molecules are able to penetrate toward the metal atom between its sandwiching ligands, as shown in Figure 2a,b (this is an important point which will come up again in the comparison of the crystals of monoclinic ferrocene and nickelocene below). A similar feature had been already observed in crystals of $(C_6H_6)_2Cr$ where six benzene ligands are able to penetrate toward the metal atom.[3c] In this context, it is noteworthy that while the ES of $(C_6H_6)_2Cr$ is made up of 12 molecules in a cubooctahedral (i.e. closest-packed) arrangement, 12-coordination is not achieved with the cyclopentadienyl ligands, i.e. with fragments having 5-fold rather than 6-fold symmetry.

In order to investigate the relationship between the two forms, let us take the central layer for reference. From Figure 3a,b, it can be easily appreciated that the main difference between the MO and OR forms is in the relative orientation of the molecular axes which form an angle of

Table II. Comparison of Potential Energy Barriers and Activation Energies (kcal mol^{-1}) for Cp Ring Reorientation in Solid Ferrocene, Nickelocene, and Ruthenocene

	ΔE(ppe)	ΔE(adp)[a]	E_a ^{1}H NMR	others
		$(C_5H_5)_2Fe$		
monoclinic 298 K[7a,b]	2.0	1.1 (2)		IQENS[15,c]
monoclinic 173 K[7a,b]	2.2	0.6 (1)	1.3 (1)[12]	1.1 (1)
triclinic[d]	2.6	1.8 (2)	1.8 (1)[12]	
101 K[6]	4.4	2.9 (5)	2.5 (1)–2.6 (5)[14]	IQENS[15,c]
	2.4	2.0 (1)		2.2
	3.4	2.1 (5)	2.0[13a]	
orthorhombic[e]	5.2	5.5 (5)		
98 K[5]	10.1	7.9 (4)	5.9 (2)[14]	
		$(C_5H_5)_2Ni$		
monoclinic 293 K[8]	1.5	1.2 (1)		RAMAN[11] 1.2
monoclinic 101 K[8]	3.3	1.6 (1)		IQENS[16,c] 1.5
		$(C_5H_5)_2Ru$		
orthorhombic[e]	3.4	5.7 (2)		
293 K[9]	8.1	9.1 (3)	2.3 (2)[12]	
orthorhombic	4.1	6.0 (2)	4.5[13a]	
101 K[9]	11.4	>12		

[a] From ref 10. [b] Refinement procedure A. [c] IQENS = incoherent quasi-elastic neutron scattering. [d] Four independent Cps. [e] Two independent Cps.

ca. 90° in the MO form while the angle is ca. 120° in the OR form. A possible pathway for the OR → MO phase transition can now be envisaged: as shown in Chart II, if the molecules of one row (e.g. molecules 7 and 6 in the orthorhombic layer) are allowed to rotate in a clockwise direction, the molecules of the neighboring row (molecules 10, 1, and 11) are forced to move in the opposite rotameric direction. The motion can propagate in the same way to the third row (molecules 9 and 8) and so forth. Altogether the process can be seen to proceed via a sort of geared rotation of the molecule within the layers, accompanied by the conformational change from eclipsed to staggered. This model implies shifts of the molecular centers along the cell axes in order to avoid repulsion between parallel molecules [the intermetal separation *increases* from 6.987 (6) (the *a* axis in the OR form) to 7.572 (4) Å (the *b* axis in the MO)] and to maintain cohesion between molecules belonging to different rows [the intermetal separation *decreases* from 12.196 (5) (the *c* axis in the OR form) to 10.443 (5) Å (the *a* axis in the MO form)]. The reorganization within the layer causes a redistribution of the dimples over the surface in which molecules belonging to the outer layers must be accommodated. As shown above, the loss in interlayer cohesion upon increase of the separation between the layers on passing from the OR to MO form is almost exactly compensated for by the gain in intralayer energy.

Relationship between the Monoclinic and Triclinic Phases of Ferrocene and the Negative Expansion Coefficient of Nickelocene. It is well-known that the crystals of monoclinic ferrocene and nickelocene show very different behaviors upon cooling. Monoclinic ferrocene undergoes a phase transition at 164 K[17] to a triclinic crystal containing two independent molecules in the asymmetric unit, which both deviate ca. 9° from the exact eclipsed orientation (see Chart I).[6] Monoclinic nickelocene, on the contrary, can be cooled down to 101 K without undergoing a phase transition.[8] In nickelocene, however, while the *a* and *c* axes show the expected shortening on passing from 293 to 101 K [10.735 (3), 10.461 (9); and 5.910 (2), 5.757 (5) Å, respectively], the *b* axis becomes longer [7.868 (3) versus 8.041 (9) Å, respectively].

Table III. Contacts (Å) for Figure 4

	ferrocene		nickelocene	
	298 K	173 K	293 K	101 K
M···H2B	3.84	3.76	3.80	3.71
M···M	5.92	5.84	5.91	5.76
H2···H5	2.45	2.42	2.54	2.51
H2···H3B	2.44	2.40	2.61	2.49
H3···H5	2.85	2.78	2.93	2.82

Table IV. Contacts (Å) for Figure 5

	ferrocene 98 K	ruthenocene 101 K
M···H5B	3.30	3.20
M···H3B	3.47	3.38
M(1)···M(4,5)	5.82	5.75
M(1)···M(2,3)	5.57	5.52
H5B···H3	2.56	2.58
H5B···H6	2.55	2.67
H3B···H3	2.48	2.64
H3B···H6	2.54	2.55

Table V. Contacts (Å) for Figure 6

Figure 6 top		Figure 6 bottom	
Fe···Fe	5.67, 5.75	Fe···Fe	5.72, 5.72
H5···H6	2.57	H2B···H8B	2.43
H5···H10	2.52	H3B···H8B	2.56
H6···H10	2.56	H5B···H10B	2.55
H2···H3	2.50	H6B···H10B	2.48
H2···H8	2.59		
H3···H8	2.57		

In the following, it will be demonstrated that these behaviors can be rationalized in terms of the relationship between molecular size and intermolecular nonbonding interactions.

As shown above, the most relevant contribution to ppe in the monoclinic crystals of the two species is given by the two molecules (separated by a cell axis translation) which are parallel to the RM and able to penetrate with their Cp ligands the hollow region around the metal atom. Figure 4 shows the pattern defined by the shortest intermolecular H···H contacts between the RM and these two neighboring molecules in the MO structure. A comparison of some relevant intermolecular distances is reported in the figure caption. It can be observed that (i) M···H and M···M distances are slightly longer in ferrocene than in nickelocene; (ii) the H···H contacts, on the contrary, are noticeably shorter in ferrocene than in nickelocene (this is true also at low temperature, even though ferrocene was measured at 173 K and nickelocene at 101 K); and (iii) as the temperature decreases, the M···H, M···M, and H···H distances show a congruent decrease.

The *intermolecular* differences outlined in (i) and (ii) are related to the small but significant difference in inter-ring separation between the two *molecular* structures. This separation is larger in nickelocene [3.64 Å] than in ferrocene [3.30 Å] so that the closeness of the Cp rings in this latter species prevents the Cp rings of molecules 2 and 3 (see Figure 4) from "pushing in" toward the metal to the extent observed in nickelocene. Since the short H···H contacts are grouped along the interlayer direction (i.e. roughly along the *c* axis), it is not surprising to observe that while the *a* and *b* axes of the MO cell of ferrocene are shorter than those of nickelocene [at 293 K: 10.530 (8) versus 10.735 (3); 7.604 (5) versus 7.868 (3) Å], the *c* axis is longer [5.921 (4) versus 5.910 (2) Å]. Very likely, at 173 K in ferrocene the H···H interactions (note H2···H5 = 2.42 Å, H2···H3B = 2.40 Å) have reached a limiting value:

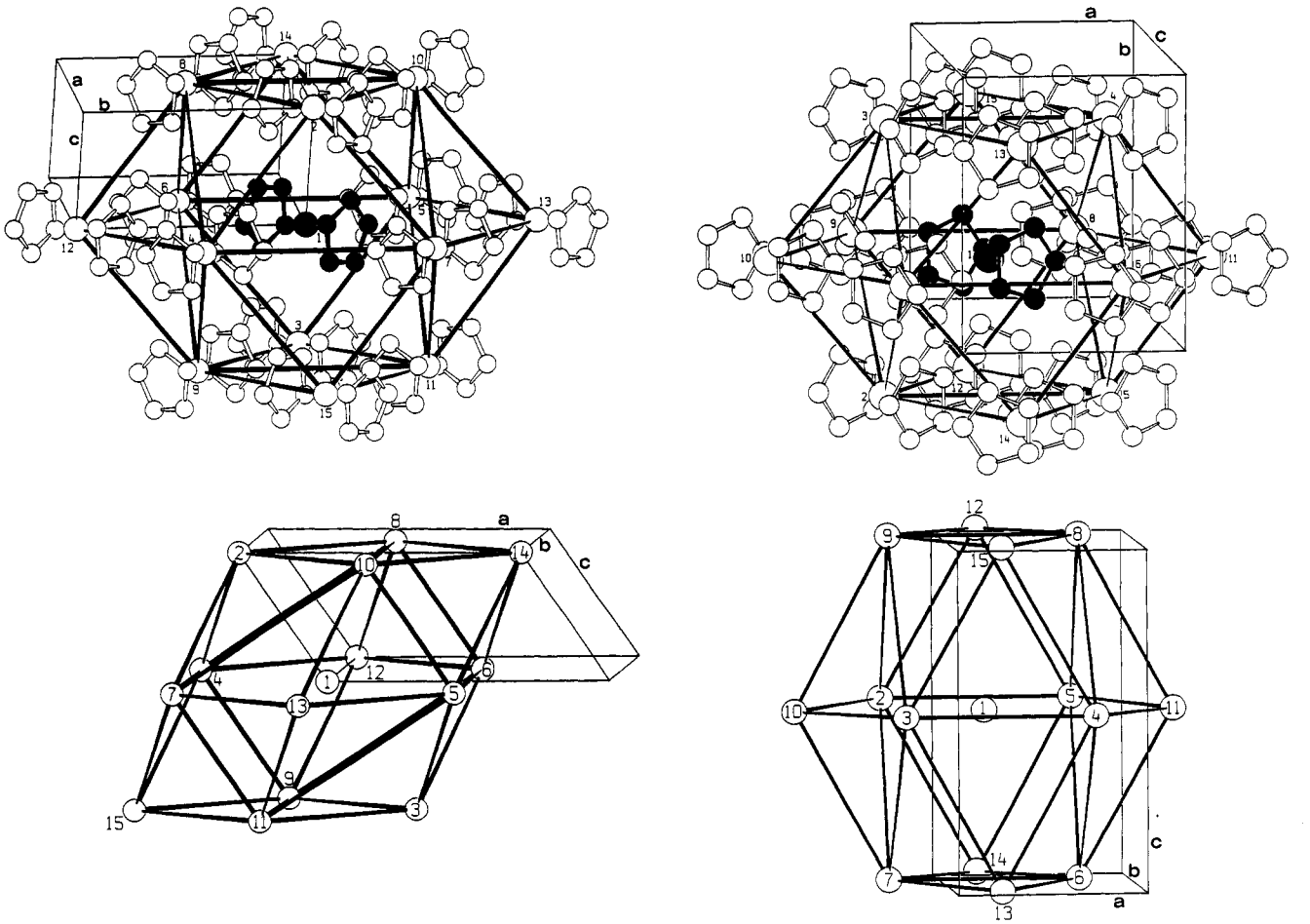

Figure 1. Enclosure shells (ESs) of monoclinic (a, top left) and orthorhombic (b, top right) ferrocene showing the distribution of the 14 first neighboring molecules. The orientation of the unit cell axes are also shown. The numbering of the molecules refers to the symmetry operation which generates the two ESs from the respective RMs (energy contribution to ppe and corresponding symmetry operations are available as supplementary material). (c and d, bottom left and right) alternative views of the monoclinic and orthorhombic ESs showing the different layer stacking sequences.

further shortening would cause loss of cohesion due to the upsurge of relevant repulsions (see below).

At this stage one may object that, since our model disregards the presence of disorder in the MO form of ferrocene[7b] (*see above*), some intramolecular contacts do not actually occur. While this is true, the objection does not change our conclusions: even if, because of disorder, some intermolecular contacts were actually slightly longer (or shorter) than those calculated for the ordered structure, their decrease with temperature would not change, nor would the inter-ring separation on which our reasoning is based. This is substantiated by the analogous situation observed in orthorhombic ferrocene[5] and orthorhombic ruthenocene,[9] which are not affected by disorder. The pattern defined by the shortest H···H contacts between the RM and the four neighboring interlocked molecules in these orthorhombic crystals is shown in Figure 5. A comparison of the two crystal structures reveals the following considerations: (i) the molecular size of ruthenocene (in terms of inter-ring separation) is larger than that of ferrocene (3.62 versus 3.31 Å) and strictly comparable with that of nickelocene; (ii) the *a* and *c* axes of orthorhombic ferrocene are smaller than in ruthenocene [6.987 (6), 7.009 (3); 12.196 (5), 12.756 (5) Å, respectively] while the *b* axis is longer [8.995 (7) versus 8.819 (4) Å]; (iii) as reported in the caption of Figure 5, M···M and M···H separations are longer in ferrocene than in ruthenocene, while H···H contacts are shorter. This is a clear indication that in ruthenocene the Cp ligands can penetrate more toward the metal atom than in ferrocene along the *b* direction, though maintaining longer H···H contacts.

Along this line of thinking it is not difficult to see that the phase transition of ferrocene toward the triclinic form at 164 K very likely arises because of the need to preserve optimum (i.e. not repulsive) H···H interactions. As a matter of fact, the torsion of the Cp ligands from the staggered conformation in the monoclinic phase, accompanied by small "adjustments" of the relative molecular orientations (so as to lead to two independent molecular units in the triclinic phase) achieve the important result of moving the H atoms of the interlocked molecules farther away, as shown in Figure 6. The closest neighbor H···H contacts, (which are ca. 2.40 Å at 173 K) lengthen to about 2.50 Å in the triclinic phase thus "relieving" the crystal packing from otherwise unacceptable repulsions.[23] A similar explanation, based on the increase of intermolecular H···H repulsions on decreasing the temperature, has been previously put forward to account for the disorder and phase transition in crystalline $(C_4H_4S)Cr(CO)_3$.[24] In es-

(22) Gavezzotti, A.; Simonetta, M. *Acta Crystallogr., Sect. A* 1976, *A32*, 997.

(23) An indirect support to this hypothesis can be gained by *calculating* the hypothetical crystal structure of a staggered monoclinic ferrocene molecule at 101 K, from the determinations at 298 and 173 K, by assuming linear dependence of the cell axes on the temperature. The computer program OPEC has an option which allows calculation of the atomic coordinates in any lattice given the known molecular geometry as input. In the model monoclinic cell the contacts H2···H5 and H2···H3B (see Figure 4) become 2.32, and 2.36 Å, respectively.

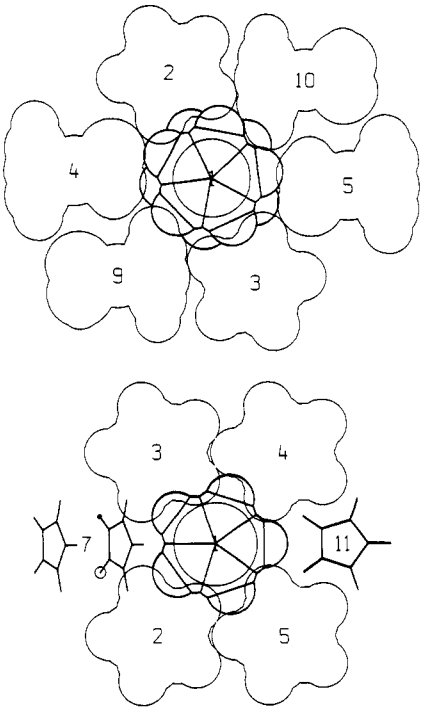

Figure 2. Sections through the Fe atom and parallel to the Cp rings of the RM in monoclinic (a, top) and orthorhombic (b, bottom) ferrocene showing how the surrounding molecules penetrate between the Cp ligands of the RM (thick space-filling outline). Numbering is as in Figure 1. Molecules 7 and 11 in (b) are above and below the grid plane.

sence, the fact the ferrocene undergoes a phase transition at 164 K while nickelocene does not is due to the effect on the intermolecular interactions of the differences in molecular size between the two species.

A rationalization of the peculiar lengthening of the *b* axis in nickelocene upon cooling can now be attempted. The temperature decrease causes a decrease in interlayer spacing (from 5.0 Å at 293 K to 4.80 Å at 101 K].[25] This is accompanied by a small torsion of the molecules in the layers (the angle formed between the molecular axis and the *ab* plane changes from 2.2 to 4.7°). This process would bring closer together the H atoms facing each other along the *b* direction if it were not accompanied by a lengthening of the *b* axis. This all is substantiated by noticing that, at 293 K, the intermolecular H1···H1B contact distance is already very short (2.40 Å, see Figure 7) and does not decrease further on cooling (2.41 Å at 101 K). If the *b* axis were to follow a "normal" thermal behavior, this very interaction would cause the upsurge of strong repulsions (computed distance for an hypothetical 2.5% decrease of the *b* axis length: 2.34 Å). In other words, the lengthening of the *b* axis compensates for the decrease in interlayer spacing, avoiding unfavorable interactions and loss of cohesion.[26]

Finally, one may wonder why the crystal structures (and packings) of nickelocene and ruthenocene are different

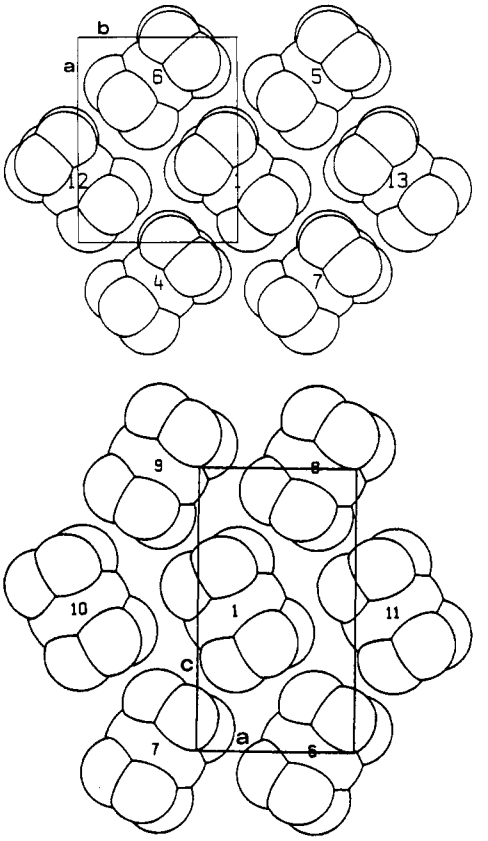

Figure 3. Ferrocene, space-filling projection of the molecules belonging to the ES equatorial plane for the MO (a, top) and OR forms (b, bottom). The molecular axes form an angle of ca. 90° in the MO form and of ca. 120° in the OR form. Numbering is as in Figure 1; H atoms are omitted for clarity.

although the inter-ring distances for the two molecules are very similar. It may well be that this difference arises from an "intrinsic" preference of these two molecules for one conformation or the other[5] (or from packing effects more subtle than those discussed thus far). Unfortunately, a conclusive answer to this question cannot be given in the absence of information on the barrier to *internal rotation* in ruthenocene.

Cyclopentadienyl Ring Reorientation in the Solid State. The potential energy barriers to ring reorientation obtained by means of the atom–atom pairwise potential energy method [ΔE(ppe)] for all species discussed herein are compared in Table II with the values derived from the anisotropic displacement parameters [ΔE(adp)] and with the potential barriers/activation energies obtained by various spectroscopic techniques. As can be seen, all sources of dynamic information are in accord in indicating that facile ring reorientation is a general feature of these metallocene crystals.

The following observations can also be made: (i) there is a generally good fit between ΔE(ppe) and ΔE(adp); (ii) while ΔE(adp) values in some cases (monoclinic ferrocene, ruthenocene) do not show the expected increase with decreasing temperature, ΔE(ppe) values show invariably a congruent behavior; (iii) it is true however that ΔE(ppe) values appear to overestimate, on the whole, the reorientational barriers (probably because of the "static environment" approximation[22]); this effect is particularly noticeable in the case of monoclinic ferrocene[7] where the comparison is most certainly complicated by the disorder which, very likely, causes the ring adp's to be anomalously large; (iv) ΔE(ppe) values compare well with the activation energies (E_a) derived from spin–lattice proton relaxation

(24) Calvarin, G.; Berar, J. F.; Weigel, D.; Azokpota, C.; Pommier, C. *J. Solid State Chem.* **1978**, *25*, 219.

(25) The interlayer spacing *d* is related, through the monoclinic angle, to the *c* axis ($d = c \sin \beta$).

(26) At this point, one may wonder why a similar effect is not observed in ferrocene. The reason is probably due to the fact that in monoclinic ferrocene, in spite of the smaller molecular size, the spacing between the molecular layers is larger than in nickelocene and decreases less on decreasing the temperature (ferrocene 5.08 Å at 298 K, 4.99 Å at 173 K, 4.90 Å at 101 K, taking half of the triclinic cell *c* axis as a measure of the pseudomonoclinic cell at this temperature; nickelocene 5.04 Å at 293 K, 4.80 Å at 101 K).

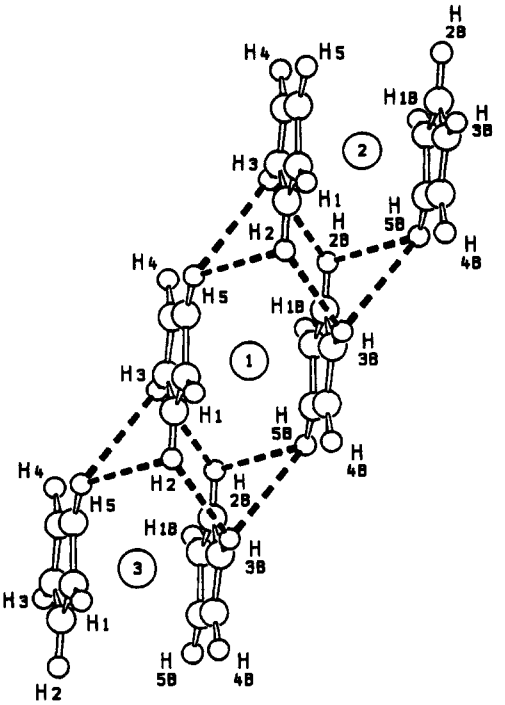

Figure 4. Representation of the shortest contacts between the RM and the closest neighboring molecules in the monoclinic crystals of ferrocene and nickelocene (numbering as in Figure 1a). The label B indicates atoms generated by the crystallographic centers of symmetry in the space group $P2_1/a$. See Table III for contact values.

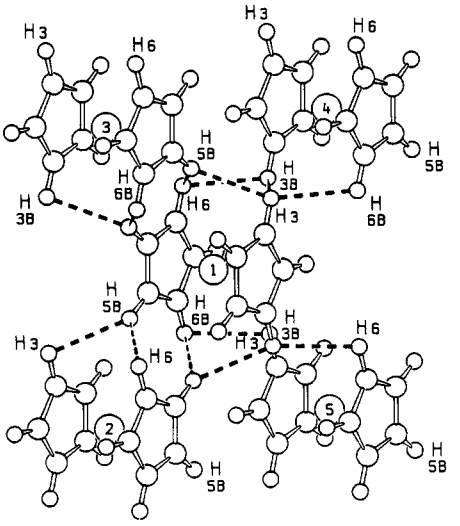

Figure 5. Representation of the shortest contacts between the RM and the closest neighboring molecules in the orthorhombic crystals of ferrocene and ruthenocene (numbering as in Figure 1b). The label B indicates atoms generated by the crystallographic centers of symmetry in the space group $P2_1/a$. See Table IV for contact values.

measurements, even though these latter values, measured over broad temperature ranges, integrate several effects (such as correlated and uncorrelated jumping motion and intramolecular energy terms) which are not accounted for in ΔE(ppe) calculations. (v) ΔE(ppe) values, as well as ΔE(adp) values, give separate barriers for crystallographically independent rings, which are not discriminated by other methods.

On these premises, it seems possible to conclude that, in the cases of low reorientational barriers, ΔE(ppe) calculations afford a rather "handy" and reliable method to explore dynamic behaviors in the solid state.

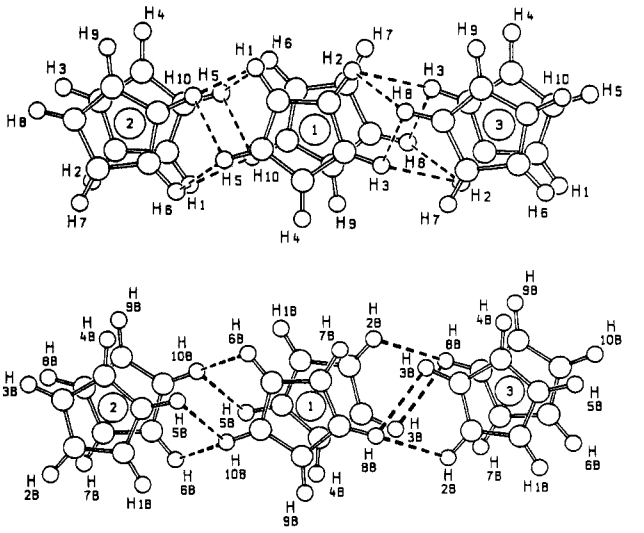

Figure 6. Representation of the shortest contacts between the two independent RMs and their closest neighboring molecules in the triclinic crystal of ferrocene. The label B indicates the second independent molecule and its closest neighboring ones (only H···H contacts below 2.6 Å are considered). See Table V for contact values.

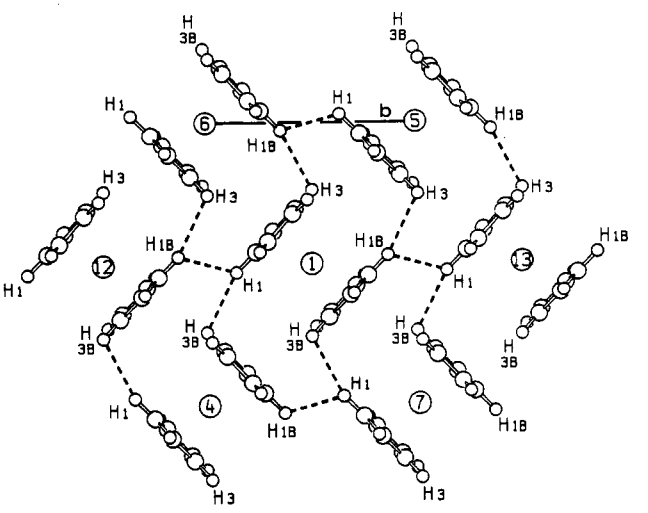

Figure 7. Representation of the shortest H···H contacts between the RM and the closest neighboring molecules in the *ab* plane in the lattice of the nickelocene (at 293 K H1···H1B = 2.40, H1···H3B = 2.62 Å; at 101 K H1···H1B = 2.41, H1···H3B = 2.56 Å). Numbering is as in Figure 1a; the label B indicates the atoms generated by the crystallographic centers of symmetry in the space group $P2_1/a$.

Summary and Conclusions

In this paper a detailed study of the relationship between the *crystal* and *molecular* structure of ferrocene, nickelocene, and ruthenocene has been carried out. We have shown that much can be learned about the properties of the metallocene crystals by studying how *shape*, *size*, and *geometry* of the molecules control the intermolecular interaction pattern and the molecular organization in the solid state. In summary we have found that (i) in spite of the differences in conformation, site symmetry, and space group symmetry, the crystal packing of the various forms of ferrocene (and therefore of nickelocene and ruthenocene) is very similar (the energy difference (from a rather crude estimate of the van der Waals packing energy) between the monoclinic and orthorhombic forms is also very small); (ii) the examination of the molecular sur-

roundings in the monoclinic and orthorhombic crystals of ferrocene affords a simple model, based on geared rotational displacements of the molecules, to explain the phase transition at 242 K; (iii) the monoclinic → triclinic transition in ferrocene arises as a consequence of the need to preserve optimum (i.e. not repulsive) H···H intermolecular interactions at temperatures below 164 K (this is achieved by adopting, in agreement with the small barrier to internal rotation, an intermediate conformation between the eclipsed and staggered forms); (iv) this behavior is not observed in monoclinic nickelocene because the larger inter-ring separation allows easier interpenetration of the neighboring interlocked molecules than in ferrocene (similar dependence of the crystal features on the molecular size is observed on comparing the intermolecular contacts in orthorhombic ferrocene and ruthenocene); (v) the negative expansion coefficient along the *b* axis in monoclinic nickelocene can also be justified on the basis of the need to avoid repulsions between the H atoms belonging to neighboring molecules separated by a cell translation; (vi) the Cp reorientational barriers calculated by means of the atom–atom potential energy method are found in good quantitative agreement with the values of the activation energies/potential barriers obtained by spectroscopic techniques or from the anisotropic displacement parameters coming from diffraction studies.

In conclusion, the different behavior of the metallocene crystals upon cooling appears to be the result of the balance between two, not necessarily converging, factors: the striving for cohesion and the need to avoid the upsurge of "localized" repulsions. Although the metallocene molecules have nearly identical shapes (and therefore pack in nearly identical ways in their solids), there are subtle differences in size and geometry which come into play when the molecules are moved closer together as the temperature is decreased. The result is a rather dramatic change in the physical properties of these otherwise extremely similar materials.

Acknowledgment. We thank Prof. A. Gavezzotti and Dr. T. F. Koetzle for their interest in this work and Dr. S. Righi for assistance with the calculations. Financial support by Ministero dell'Università e della Ricerca Scientifica e Tecnologica is acknowledged.

Registry No. $(C_5H_5)_2Fe$, 102-54-5; $(C_5H_5)_2Ni$, 1271-28-9; $(C_5H_5)_2Ru$, 1287-13-4; cyclopentadiene, 542-92-7.

Supplementary Material Available: A listing of the symmetry operations generating the ESs and of the individual contribution to ppe of each ES molecule (1 page). Ordering information is given on any current masthead page.

Organometallic Intermediates in Dehydrobrominations Catalyzed by Metals and Metal Bromides

Angela R. Suárez,* Alejandra G. Suárez, and María R. Mazzieri

Departamento de Química Orgánica, Facultad de Ciencias Químicas, Universidad Nacional de Córdoba, 5016 Córdoba, Argentina

Received September 30, 1991

Iron, ruthenium, aluminum, and their anhydrous bromides were used as catalysts for dehydrobromination of 1,2-dibromo-1,1-diphenylethane in carbon tetrachloride solutions to give 2-bromo-1,1-diphenylethene. Organometallic species formed on the surface of the solid catalysts moved into the solution and were detected spectroscopically. The reactivity of the studied catalyst was Al < $AlBr_3$ ≈ Ru < $RuBr_3$ < $FeBr_2$ ≈ $FeBr_3$ ≈ Fe.

Introduction

Hydrogen halide abstraction from alkyl halides can be achieved under several conditions. Nevertheless, there is little work on dehydrohalogenation catalyzed by transition-metal compounds in the condensed phase, and the mechanism is still unclear. Synthetic applications of hydrogen halide elimination from alkyl halides mediated by nickel complex were reported by Smith et al.[1]

In a previous paper we reported the dehydrohalogenation of 1,2-dibromo-1,1-diphenylethane in carbon tetrachloride solutions catalyzed by powdered iron.[2] We isolated stable organoiron compounds and detected organometallic intermediates that after being formed on the metal surface moved into the solution that changed from colorless to red-brick. Steps proposed for the reaction involved the well-known oxidative addition and β-elimination, both very common pathways in many catalytic processes involving organometallic systems. Scheme I shows the mechanism.

Scheme I

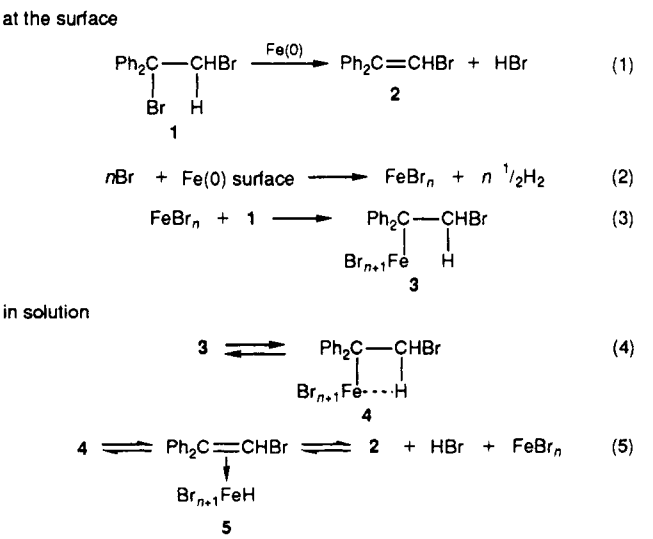

The participation of such organometallic intermediates was detected in several ways. Electronic absorption spectra

(1) Henningsen, M. C.; Jeropoulos, S.; Smith, E. H. *J. Org. Chem.* **1989**, *54*, 3015.
(2) Suárez, A. R.; Mazzieri, M. R.; Suárez, A. G. *J. Am. Chem. Soc.* **1989**, *111*, 763.

0276-7333/92/2311-0718$03.00/0